The following article is a pre-print of:

Stilgoe, Alexander B., Nieminen, Timo A. and Rubinsztein-Dunlop, Halina "Energy, momentum and propagation of non-paraxial high-order Gaussian beams in the presence of an aperture." Journal of Optics, 17(12): 125601, 2015.

doi:10.1088/2040-8978/17/12/125601

Energy, momentum and propagation of non-paraxial high-order Gaussian beams in the presence of an aperture

Alexander B Stilgoe[1], Timo A Nieminen[1], Halina Rubinsztein-Dunlop[1]

[1]School of Mathematics and Physics, The University of Queesnland, The University of Queensland, St. Lucia, QLD, 4072, Australia.

email: a.stilgoe@uq.edu.au

Abstract

Non-paraxial theories of wave propagation are essential to model the interaction of highly focussed light with matter. Here we investigate the energy, momentum and propagation of the Laguerre–, Hermite– and Ince–Gaussian solutions (LG, HG, and IG) of the paraxial wave equation in an apertured non-paraxial regime. We investigate the far-field relationships between the LG, HG, and IG solutions and the vector spherical wave function (VSWF) solutions of the vector Helmholtz wave equation. We investigate the convergence of the VSWF and the various Gaussian solutions in the presence of an aperture. Finally, we investigate the differences in linear and angular momentum evaluated in the paraxial and non-paraxial regimes. The non-paraxial model we develop can be applied to calculations of the focusing of high-order Gaussian modes in high resolution microscopes. We find that the addition of an aperture in high numerical aperture optical systems does not greatly affect far-field properties except when the beam is significantly clipped by an aperture. Diffraction from apertures causes large distortions in the near-field and will influence light-matter interactions. The method is not limited to a particular solution of the paraxial wave

equation. Our model is constructed in a formalism that is commonly used in scattering calculations. It is thus applicable to optical trapping and other optical investigations of matter.
PACS: 02.30.Gp, 42.25.Bs, 42.60.Jf, 87.80.Cc

1 Introduction

Recently there has been growing interest in optical trapping of functional solids [1] and topological (dis-)order in paraxial wave optics [2, 3]. Transverse modes of light can be simply derived in the paraxial regime, but no simple representation exists for the highly focused beam cases in the presence of an aperture.

Solutions of both paraxial and non-paraxial wave equations can be written down in the form of a sum over a complete basis of orthogonal wave functions, such as:

$$E\left(\mathbf{r},t\right)=e^{-\mathrm{i}\omega t}\sum_{i}a_{i}\psi_{i}\left(\mathbf{r}\right), \tag{1}$$

where a_i is the complex amplitude of wave function ψ_i which is a function of spatial coordinates $\mathbf{r}$. Wave function expansions of this sort have excellent properties, such as orthogonality, compact form or discreteness of the basis. For particular coordinate systems the wave functions ψ_i can be obtained by separation of variables of the differential equation. For the paraxial wave equation, the best known orthogonal modes are the Laguerre–Gaussian (cylindrical coordinates) and Hermite–Gaussian (Cartesian coordinates) modes, which can be thought of as limiting cases of the Ince–Gaussian (elliptical coordinates) modes [4].

The vector Helmholtz differential equation can be written as:

$$\nabla^{2}\mathbf{\Psi}+k^{2}\mathbf{\Psi}=0, \tag{2}$$

where ∇^2 is the vector Laplacian and $\mathbf{\Psi}$ is a vector field wave solution. One of the best known examples of solutions of the scalar Helmholtz wave equation are the spherical harmonics, which is used to model monochromatic non-paraxial scalar waves such as sound. For the vector wave equivalent, the vector Helmholtz equation, vector spherical wave functions (VSWFs) are used to model monochromatic vector wave propagation. In spherical coordinates, (r,θ,ϕ), this vector problem is separable using a technique that employs the scalar wave function solution as a seed function to generate the orthogonal vector basis [5]. The orthogonal vector basis is a set of VSWFs. As the VSWFs are separable into angular and radial components and the

radial components are a simple spherical wave far from the origin. These functions have features highly suited for representations of highly-focused beams and allow a purely angular representation of beams which simplified the problem of finding the weighting for the basis. The angular vector components of the VSWFs are known as the vector spherical harmonics (VSHs) and can be defined as [6]:

$$\mathbf{B}_{nm} = \hat{\theta}\frac{\partial}{\partial\theta}Y_n^m(\theta,\phi) + \hat{\phi}\frac{\mathrm{i}m}{\sin\theta}Y_n^m(\theta,\phi), \tag{3}$$

$$\mathbf{C}_{nm} = \hat{\theta}\frac{\mathrm{i}m}{\sin\theta}Y_n^m(\theta,\phi) - \hat{\phi}\frac{\partial}{\partial\theta}Y_n^m(\theta,\phi), \tag{4}$$

$$\mathbf{P}_{nm} = \hat{r}Y_n^m(\theta,\phi), \tag{5}$$

where $\hat{r}$, $\hat{\theta}$, and $\hat{\phi}$ are the spherical unit vector components, Y_n^m is the spherical harmonic of degree, n, and order, m. Infinite superpositions of these vector spherical harmonics can generate arbitrarily shaped time harmonic electromagnetic fields in the far-field. $\mathbf{B}_{nm}$ and $\mathbf{C}_{nm}$ form a complete basis for a propagating linear time-harmonic vector wave in the far-field. A superposition of these wave functions yields the far-field electric and magnetic field which are:

$$\lim_{r\to\infty}\mathbf{E}(r,\theta,\phi,t) = e^{-\mathrm{i}\omega t}h_0^{(2)}(kr)\sum_{n,m}\frac{\mathrm{i}^n}{\sqrt{n(n+1)}} \times\left(a_{nm}\mathbf{C}_{nm}(\theta,\phi) - \mathrm{i}b_{nm}\mathbf{B}_{nm}(\theta,\phi)\right), \tag{6}$$

$$\lim_{r\to\infty}\mathbf{H}(r,\theta,\phi,t) = e^{-\mathrm{i}\omega t}\frac{h_0^{(2)}(kr)}{iZ}\sum_{n,m}\frac{\mathrm{i}^n}{\sqrt{n(n+1)}} \times\left(-\mathrm{i}a_{nm}\mathbf{B}_{nm}(\theta,\phi) + b_{nm}\mathbf{C}_{nm}(\theta,\phi)\right), \tag{7}$$

for inward propagating spherical waves where $h_0^{(2)}$ is a spherical Hankel function [7, 8] of the second kind of degree 0, Z is the impedance of the medium, and a_{nm} and b_{nm} are the complex weights for the wavefunctions corresponding to transverse electric (TE) and transverse magnetic (TM) modes.

The far-field momentum properties of paraxial modes can be expressed analytically in the VSWF for unapertured (i.e. not travelling through a pupil) Gaussian–type modes [9]. This is because Laguerre–, Hermite– and Ince–Gaussian (henceforth, LG, HG and IG) modes, like the functions which define the spherical harmonics, are hypergeometric functions in the far-field. The conversions between these forms can be calculated with algebraic relations [8]. However, in an actual optical system these analytical solutions cannot always be used because such systems contain apertures which introduce edge effects. In the presence of an aperture the mode weights can

be found by integral transform over a spherical surface, defined by some solid angle surface ω, where:

$$a_{nm} = \frac{\mathrm{i}^n}{\sqrt{n(n+1)}} \int_\omega \mathbf{C}^\star_{nm}(\theta,\phi) \cdot \mathbf{A}(\theta,\phi)\, \mathrm{d}\Omega, \tag{8}$$

$$b_{nm} = \frac{\mathrm{i}^{n-1}}{\sqrt{n(n+1)}} \int_\omega \mathbf{B}^\star_{nm}(\theta,\phi) \cdot \mathbf{A}(\theta,\phi)\, \mathrm{d}\Omega, \tag{9}$$

where wavefunctions $\mathbf{C}^\star_{nm}$ and $\mathbf{B}^\star_{nm}$ are complex conjugated VSHs, $\mathrm{d}\Omega$ is the solid angle infinitesimal, $\mathbf{A}$ is the amplitude of a time-harmonic electromagnetic spherical wave as a function of angle in the far-field, such that

$$\lim_{r\to\infty} \mathbf{E}(r,\theta,\phi,t) = e^{-\mathrm{i}\omega t}\mathbf{A}(\theta,\phi)\, h_0^{(2)}(kr). \tag{10}$$

One could also reform these integral transforms, equations (8) and (9), into a linear algebra problem and use a standard linear matrix solver which has shown excellent convergence [10] and has been successfully used for the modelling of beams used in optical tweezers [11].

To solve for the mechanical properties of propagating radiation we will also need to calculate the linear and angular momentum obtained from the distribution of radiation. The linear and angular momentum of the vector spherical harmonic waves under the action of the linear and angular momentum operators have been calculated and have analytical solutions [12, 13]. In our work we will use this derived result to calculate the spin and total angular momentum of electromagnetic waves.

In this article we first investigate the relationship between the symmetries of high-order Gaussian beams and the VSH in the far-field where we also start constructing our electromagnetic propagation model. We follow this with a formalism of the relationships between different types of high-order Gaussian beams showing how to construct the vortex Ince–Gaussian beam modes from Laguerre–Gaussian beam modes. We also integrate the transformation matrix into our non-paraxial formalism to generate the non-paraxial Ince–Gaussian beam modes. We then investigate the energy distribution of non-paraxial modes based on high-order Gaussian beams in the presence of an aperture. We verify that we can model realistic diffraction effects via experimental investigation of an apertured Ince–Gaussian beam and compare the shape of the modes in the non-paraxial regime with those in the paraxial one. We finish the article with a discussion of the momentum properties of highly focussed high-order Gaussian beams. By investigating beams in this manner we can discuss the behaviour of paraxial modes using LG beams and their vector wave equivalent in both free-space and high resolution microscopes. Our formalism is general enough

to allow extension into the analysis of beams with non-uniform (vector) polarisation and the investigation of topologies involving rotational and mirror symmetries.

2 High-order Gaussian beams, symmetries, and the vector field

Paraxial conversions between the LG and HG beams have been studied [14, 15, 16] as well as the IG family [17]. We will discuss transformations of this sort as a general class of conversions between paraxial modes and apply them to the non-paraxial regime. In the far-field limit a beam is an angular pattern of light, regardless of its representation in any particular basis. We can define our far-field high-order Gaussian mode solving a paraxial wave equation as:

$$G_{\Lambda,i}(\theta,\phi) = \mathcal{F}_{\Lambda,i}(\theta,\phi) \times \exp\left(-f^2(\theta) \pm \mathrm{i}(\Lambda+1)\frac{\pi}{2}\right), \tag{11}$$

where $\mathcal{F}_{\Lambda,i}$ are the functions required by a particular geometry solving the paraxial wave equation, for $i = 0, ..., \Lambda$. For the fundamental Gaussian mode, $\Lambda = 0$ and $\mathcal{F}_{0,0} = 1$. For $\Lambda = 1$, $\mathcal{F}_{1,i} = \sqrt{2} f(\theta) \exp((2i - \Lambda)\mathrm{i}\phi)$ and it gives the first vortex (LG) mode. The degree (highest polynomial power within $\mathcal{F}(\theta,\phi)$) of the equation, Λ, corresponds to the Gouy phase shift. $f(\theta)$ is the function parameterising the aperture as a function of angle and the Gouy phase [18] is represented by the final factor of the exponential of equation (11). Somewhat confusingly, the mathematical term degree is interchanged with order in the field of optical physics when referring to higher-order Gaussian beams. When referring to expressions here, degree explicitly refers to the highest polynomial power of a function. In the weakly converging regime 2D diffraction theory is necessary to propagate vector solutions of the paraxial wave equation from the far-field to the near-field and to incorporate polarisation. *Post-hoc* vectorised solutions of the paraxial wave equation incorporating polarisation have led to useful physical insights [19, 20] but ultimately cannot accurately represent momentum distributions with arbitrary polarisation [9, 21, 22]. By utilising transformations between the paraxial and vector wave solutions, radial and azimuthal polarisation paraxial-like modes can be both generated and analysed for all the paraxial beam modes. Far from any scatterers the characteristics of a spherical wave traveling in infinite space are angular with respect to some arbitrary point. For a microscope the focus is a natural origin to pick for the optical system. In this formalism a simulated aperture must be defined as an angular filter. This implies

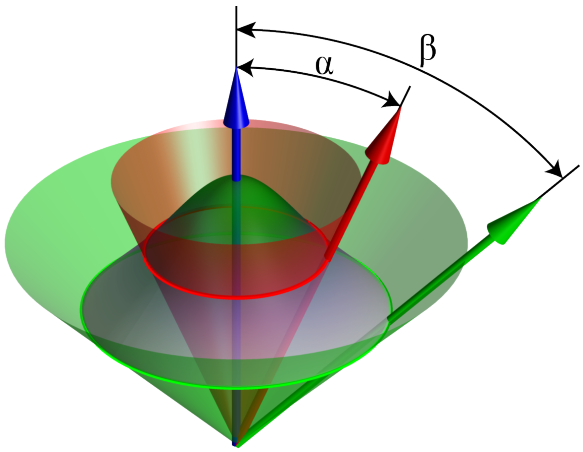

Figure 1: Graphical representation of a Gaussian beam at an aperture in the far-field. The mode in our computational model is scaled in the far-field coordinates so that two criteria are met: 1) that the far-field beam waist is situated at angle α and 2) the beam amplitude is confined to an area bounded by angle β.

that any propagating radiation can be defined as a function of angle; this includes Gaussian and high-order Gaussian beams. Figure 1 graphically demonstrates the key angular parameters used in our model for the computation of high-order Gaussian modes. α is the angle demarking the far-field beam waist (red) and β is the angle demarking the angular extent of the aperture (green). The focus (near-field) of the beam mode is where the beam waist cone (red) intersects the aperture cone (green) and the three arrows originate.

Equation (11) presents a starting point for modelling light propagation of Gaussian beams in a standard microscope. As a microscope typically has a circular aperture the edge effects we model should match those observed in experiments. Our functions corresponding to a constant Gouy phase shift require

$$\mathcal{G}_{\Lambda,i}\left(u,v\right)=\sum_{j=0}^{\Lambda}c_{ij}\mathcal{F}_{\Lambda,j}\left(\theta,\phi\right) \tag{12}$$

where $\mathcal{G}_{\Lambda,i}\left(u,v\right)$ are the beam energy normalised basis functions constructed out of our constituent orthogonal polynomials $\mathcal{F}_{\Lambda,j}$ and weights c_{ij}.

Let us now introduce the VSH. Consider a point in the far-field defined in Cartesian coordinates; by definition there are no radial components, and therefore, the

transformation in the small angle approximation is given by:

$$\begin{bmatrix} E_\theta \\ E_\phi \end{bmatrix} = \begin{bmatrix} \pm\cos\phi & \pm\sin\phi \\ -\sin\phi & \cos\phi \end{bmatrix} \begin{bmatrix} E_x \\ E_y \end{bmatrix} \tag{13}$$

which completely maps the far-field from Cartesian to spherical coordinates (for small angles). Thus we can model all kinds of arbitrarily polarised linear time-harmonic beams in spherical coordinates. This is sufficient to use as input to solve the general problem, equations (8) & (9). However, this is a time consuming and laborious process, even with numerical calculation on a modern (fast) computer. This difficulty is ameliorated by exploiting the various similarities of functions to model mirror symmetric and uniformly polarised beams. No rotational symmetry reduction can be performed for VSH as they are already an irreducible representation of rotational symmetry.

A uniformly polarised LG beam can be expressed using left and right circular polarisation components, E_{σ^+} and E_{σ^-}. Left and right components of polarisation combined with the azimuthal function $\exp(\mathrm{i}l\phi)$ correspond to: $m = l \pm 1$ in the VSH, equations (3) and (4). We can relate Jones vectors to the amount of left and right circular polarisation (in our convention the azimuthal function in our VSHs use $\exp(-\mathrm{i}m\phi)$ as the azimuthal part) components with the equations:

$$\begin{bmatrix} \mathcal{C}_{l-1} \\ \mathcal{C}_{l+1} \end{bmatrix} = \frac{(-1)^l}{\sqrt{2}} \begin{bmatrix} E_{\sigma^-} \\ E_{\sigma^+} \end{bmatrix} \tag{14}$$

$$= \frac{(-1)^l}{\sqrt{2}} \begin{bmatrix} 1 & \mathrm{i} \\ 1 & -\mathrm{i} \end{bmatrix} \begin{bmatrix} E_x \\ E_y \end{bmatrix} \tag{15}$$

where $\mathcal{C}_{l\pm1}$ is the weight of VSHs having azimuthal mode $m = l \pm 1$.

Mirror and parity symmetries for the VSH are related and can be understood by considering relations like: $2\cos m\theta = \exp(+\mathrm{i}m\theta) + \exp(-\mathrm{i}m\theta)$ or $2\mathrm{i}\sin m\theta = \exp(+\mathrm{i}m\theta) - \exp(-\mathrm{i}m\theta)$ which are angular component 'mirrors' of each other.

Our choice of vector spherical wave functions make it straightforward to model 'arbitrary' paraxial beam modes which were found in non-rotational coordinates. Generalised vector beams cannot be expressed so simply, as such a beam will in general require every mode. However, radial and azimuthally polarised beams are the radial, $\hat{r}$, and azimuthal, $\hat{\phi}$ components of VSWF and as a result have well defined interrelations to the VSH.

3 Transformations of Laguerre–, Ince–, and Hermite–Gaussian beam modes

The paraxial wave equation in elliptical coordinates is separable. Considering a transverse part of the paraxial wave equation we can treat a single separable coordinate, say z. The form of the resulting equation is that of the Ince differential equation:

$$\frac{\mathrm{d}^2\psi}{\mathrm{d}z^2} + \xi \sin 2z \frac{\mathrm{d}\psi}{\mathrm{d}z} + [\eta - \Lambda\xi \cos 2z]\,\psi = 0. \tag{16}$$

where z is the argument of ψ (or a separable transverse coordinate of the paraxial wave equation), Λ corresponds the degree of the wavefunction, ξ is the ellipticity (continuous parameter changing polar to Cartesian coordinate systems), η is an offset to the eigenvalues. Following the methodology found in [23] we can solve the Ince differential equation [24] eigenproblem. There are two classes of stationary solutions to a wave equation: a set of symmetric eigenfunctions and a set of anti-symmetric eigenfunctions. Together these wave functions can form a complete basis over the complex field and hence can also give transverse angular momentum modes. Finding the solutions for all potential functions satisfying a Gouy phase shift $(\Lambda + 1)\pi/2$ is necessary and sufficient to convert between Laguerre–, Ince– and Hermite–Gaussian beam modes.

Beijersbergen *et al.* [15] presented one of the simplest definitions of the transformation for the Hermite–Gaussain to *vortex* Laguerre–Gaussian beams using a standard formulation of the paraxial wave equation. Later, transformations of a similar kind were used to generate the HG $\leftrightarrow$ IG and the IG $\leftrightarrow$ *non-vortex* LG modes [17]. To construct the vortex IG modes a superposition of symmetric and anti-symmetric non-vortex modes can be used [17, 25]. From a symmetry perspective this is a completely satisfactory method of generating orbital angular momentum modes in the paraxial beam family as the 'cosine' and 'sine' modes are complementary and form a complete basis over the complex field. If we wish to represent the *vortex* mode conversions over the complex plane with an object, we can construct them out of vortex LG modes which have the same azimuthal symmetries as the VSWFs. In the limiting case of polar coordinates the transformation matrix should match LG modes onto themselves, thus

$$\lim_{\xi \to 0} c_{\Lambda,\xi} = \mathbb{I}_\Lambda, \tag{17}$$

where $\mathbb{I}_\Lambda$ is the identity matrix of the same size as $c_{\Lambda,\xi}$ and Λ is the degree of the orthogonal function and ξ is the ellipticity. This ensures that in the limit of no ellipticity ($\xi \to 0$) we have the original LG modes. Our transformation can be valid

when $\xi \to \infty$, because the matrix $c_{\Lambda,\xi}$ combines symmetric and anti-symmetric wave functions and is,

$$\lim_{\xi\to\infty} c_{\Lambda,\xi}(i,j) = b(\Lambda - 2i, 2i, j) + \mathrm{sgn}\,(2i-\Lambda) \times b(\Lambda - 2i - 1, 2i + 1, j), \tag{18}$$

where i and j are respectively the column and row index of c, $\mathrm{sgn}\,(2i-\Lambda) = 0$ for $\Lambda = 2i$ and $b(n,m,k)$ is defined in equation (9) of Beijersbergen *et al.* [15], n and m being replaced by a function of matrix indices i and j.

Our construction of $c_{\Lambda,\xi}$ needs to have the appropriate limits of ξ for LG and HG modes and the constituent functions must satisfy the Ince differential equation. Let us label a matrix of eigenvectors for symmetric wave functions as $A_{\Lambda,\xi}$ and the matrix of eigenvectors for anti-symmetric functions as $B_{\Lambda,\xi}$ with rows ordered by descending eigenvalue which results in matrices with dimensions of length $\lfloor \Lambda/2 + 1 \rfloor$. The matrices $A_{\Lambda,\xi}$ and $B_{\Lambda,\xi}$ will take the real and imaginary parts of rotationally symmetric modes and transform them to the real and imaginary parts of some elliptical mode. We need to re-express the matrices in a form to act on rotational modes which have both symmetric (real) and anti-symmetric (imaginary) components. Let us define $\alpha_{\Lambda,\xi}$ and $\beta_{\Lambda,\xi}$:

$$\alpha_{\Lambda,\xi} = \begin{bmatrix} A\,(i,j) & A\,(i,\Lambda - j') \\ A\,(\Lambda - i', j) & A\,(\Lambda - i', \Lambda - j') \end{bmatrix} \tag{19}$$

$$\beta_{\Lambda,\xi} = \begin{bmatrix} B\,(i,j) & -B\,(i,\Lambda - j') \\ -B\,(\Lambda - i', j) & B\,(\Lambda - i', \Lambda - j') \end{bmatrix} \tag{20}$$

where the matrix indices: $i = i' = 0...\Lambda$ and $j = j' = 0...\Lambda$ hold good for all odd Λ. In the case that Λ is even, the blocks of α and β can't be the same size as we have an *odd* number of modes. Instead: $i' = 1...\Lambda$ and $j' = 1...\Lambda$ and we also set $B_{\Lambda,j} = B^T_{i,\Lambda} = 0$ as there is one less anti-symmetric function than symmetric functions for even Λ.

We now compute the vortex mode transformation, $c_{\Lambda,\xi}$, by normalising the row vectors of $\alpha_{\Lambda,\xi}$ and $\beta_{\Lambda,\xi}$ and adding them together:

$$c_{\Lambda,\xi}\,(i,j) = \frac{\alpha_{\Lambda,\xi}\,(i,j) + \beta_{\Lambda,\xi}\,(i,j)}{\sqrt{\sum_j \left(\alpha_{\Lambda,\xi}\,(i,j) + \beta_{\Lambda,\xi}\,(i,j)\right)^2}}, \tag{21}$$

resulting in an ordered transformation matrix such that for matrix indices i and j

$$c_{5,2} = \begin{bmatrix} 0.961 & -0.270 & 0.064 & 0.016 & -0.004 & -0.002 \\ 0.260 & 0.798 & -0.508 & -0.165 & -0.103 & -0.005 \\ 0.088 & 0.504 & 0.837 & -0.101 & 0.161 & 0.040 \\ 0.040 & 0.161 & -0.101 & 0.837 & 0.504 & 0.088 \\ -0.005 & -0.103 & -0.165 & -0.508 & 0.798 & 0.260 \\ -0.002 & -0.004 & 0.016 & 0.064 & -0.270 & 0.961 \end{bmatrix}, \tag{25}$$

we have the desired superposition, equation (12), for Gaussian modes:

$$\mathrm{LG}_i = \sum_{j=0}^{\Lambda} c_{\Lambda,0}\,(i,j)\,\mathrm{LG}_j \tag{22}$$

$$\mathrm{HG}_i = \sum_{j=0}^{\Lambda} c_{\Lambda,\xi\to\infty}\,(i,j)\,\mathrm{LG}_j \tag{23}$$

$$\mathrm{IG}_i = \sum_{j=0}^{\Lambda} c_{\Lambda,\xi}\,(i,j)\,\mathrm{LG}_j \tag{24}$$

where LG modes are ordered such that the standard Laguerre–Gaussian modes are $p = (\Lambda - |\Lambda - 2i|)/2$ and $l = -\Lambda + 2i$.

Figure 2 shows the real and imaginary parts of the free-space paraxial mode field resulting from equation (25) acting on LG modes of degree 5. As the real and imaginary parts of the complex fields show, we have calculated the appropriate weightings of LG modes from the first three rows of $c_{5,2}$ to produce the IG modes. The remaining rows of the matrix are the angular momentum mirrors and will not appear any differently on this plot than the modes already displayed.

4 Non-paraxial Ince–Gaussian beams

The propagation of light and its other properties have been previously analysed and modelled with vector spherical wave functions [5, 26, 27, 7, 28]. The VSWF is a natural choice to use in modelling non-paraxial systems with circular apertures. In section 3 we have calculated the superposition of LG modes yielding the IG modes. We now construct the non-paraxial beam equivalent using VSH. Equations (8) and (9) relate a field pattern in the far-field to the VSH. If we consider only rotationally symmetric modes the 2D surface integrals become 1D integrals. As VSH are an irreducible representation of rotationally symmetric modes in the m (axial angular

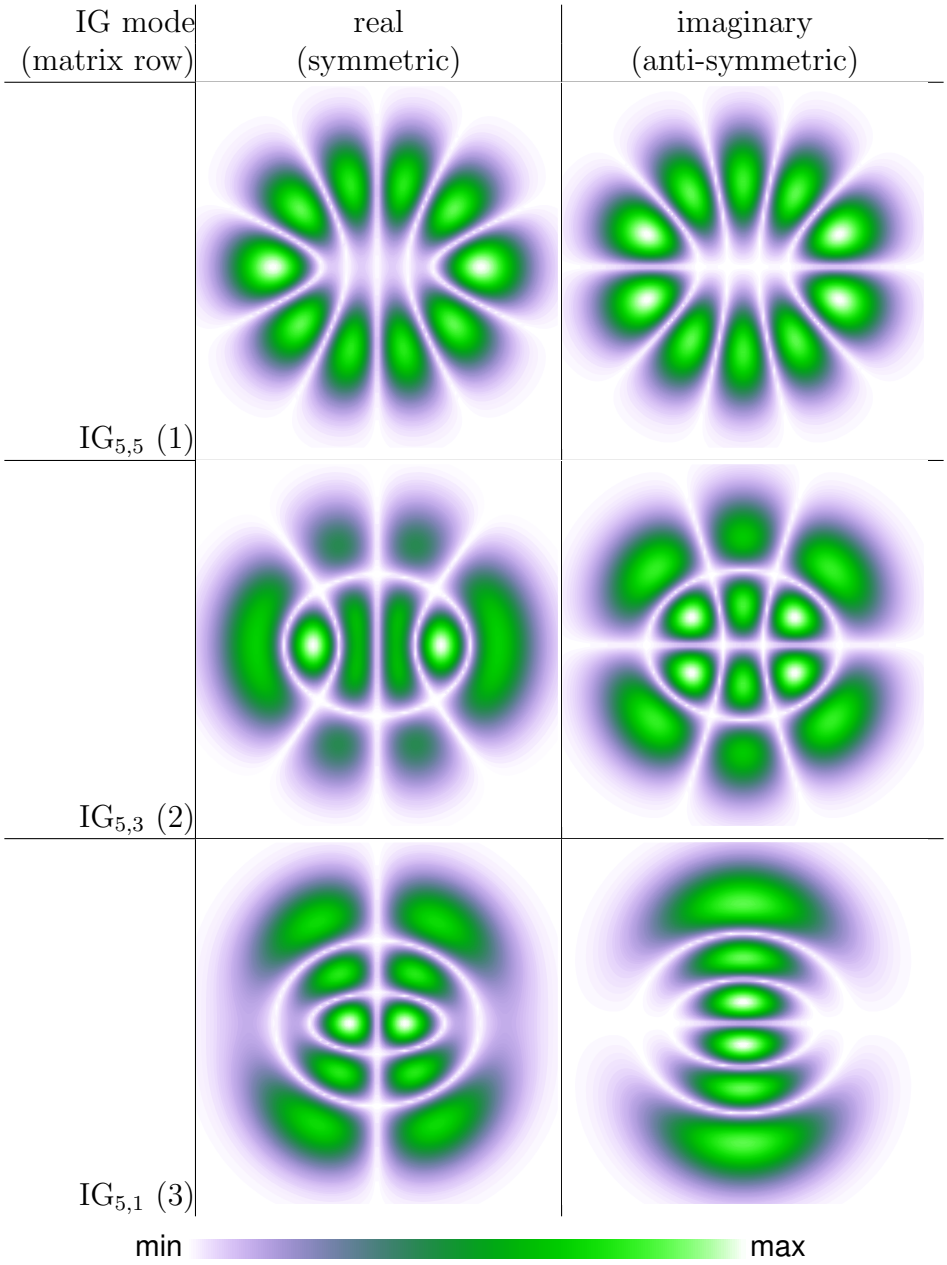

Figure 2: The magnitude of the real and imaginary parts of the scalar field of paraxial Ince–Gaussian modes generated from a superposition of LG beams weighted by the first three rows of $c_{5,2}$ (equation (25)).

momentum) index our rotationally symmetric modes have at most one component in the VSH for each 'radial' mode n. As we wish to perform calculations for a uniform polarisation, we take the $m = l \pm 1$ components of the VSH:

$$a_{n,l\pm1} = \frac{\mathrm{i}^n}{\sqrt{n(n+1)}} \int_0^\beta \mathbf{C}^\star_{n,l\pm1}(\theta, 0) \cdot \mathbf{A}(\theta) \sin\theta \mathrm{d}\theta, \tag{26}$$

$$b_{n,l\pm1} = \frac{\mathrm{i}^{n-1}}{\sqrt{n(n+1)}} \int_0^\beta \mathbf{B}^\star_{n,l\pm1}(\theta, 0) \cdot \mathbf{A}(\theta) \sin\theta \mathrm{d}\theta, \tag{27}$$

where β is the half cone angle (see figure 1) for the extent of the aperture, and we define

$$\mathbf{A}(\theta) = \left(\sqrt{2} f(\theta)\right)^{|l|} \times \mathcal{L}_p^{|l|}\left(2f^2(\theta)\right) \exp\left(-f^2(\theta)\right) \cdot \left[\hat{\theta} + \hat{\phi}\right] \tag{28}$$

and $f(\theta) = (kw_0/2) \sin\theta$.

In its current form $\mathbf{A}$ represents linearly 'x' polarised beams when integrated into the vectors $\mathbf{a}$ and $\mathbf{b}$. To rotate the polarisation around the Poincaré sphere the weights calculated from the Jones vector shown in equation (14) are used in their respective $m = l \pm 1$ modes.

We apply $c_{\Lambda,\xi}$ to our VSH representation of LG modes:

$$\mathbf{a}_i^{\mathrm{IG}} = \sum_{j=0}^{\Lambda} c_{\Lambda,\xi}(i,j)\, \mathbf{a}_j^{\mathrm{LG}} \tag{29}$$

$$\mathbf{b}_i^{\mathrm{IG}} = \sum_{j=0}^{\Lambda} c_{\Lambda,\xi}(i,j)\, \mathbf{b}_j^{\mathrm{LG}} \tag{30}$$

where $\mathbf{a}_i$ and $\mathbf{b}_i$ are the resulting sum of VSH for IG beams i from LG beams j as previously defined for equations (22–24). Any paraxial mode can be modelled given an appropriate transformation matrix. We can compare the paraxial modes calculated from figure 2 with the non-paraxial modes (again calculated with equation (25)) in figure 3. There are two effects which can be observed in the magnitude of electric field. The first effect one would note is a reduction of amplitude visible at the focus. The second effect is a reduction in visibility between the bright and dark spots in the beam profile due to the increased contribution of the axial field component. All these effects have real consequences for how the light field locally interacts and couples to matter. For example, particular regions of the beam could have large intensity gradients and hence facilitate enhanced optical trapping.

We will now show how the method described above can be used to model diffraction from an aperture. We investigate the trade off between accurate representations

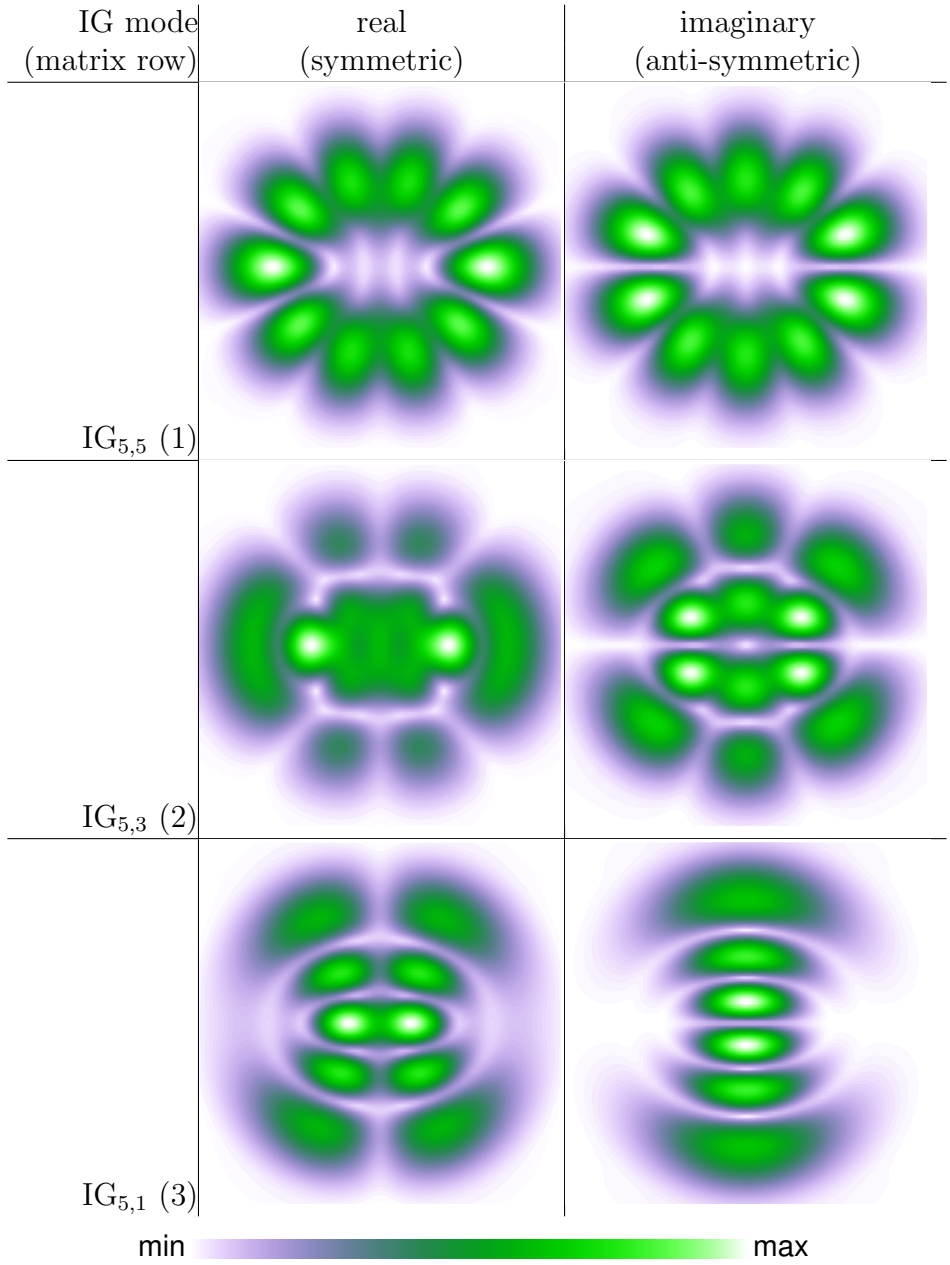

Figure 3: The magnitude of the real and imaginary parts of the electric field of non-paraxial Ince–Gaussian modes generated from a superposition of LG beams weighted by the first three rows of $c_{5,2}$.

of the beam versus the truncation of the basis for various relative aperture sizes. Paraxial high-order Gaussian beams has the time averaged energy flux fall-off proportional to the exponential part in the transverse plane, $\exp(-k^2r^2)$, we should see this in our calculation of VSWFs. The radial part of the VSWFs in our spherical wave function expansion falls off like $1/kr$ (in oscillator units kr) for large arguments and so we should see such energy flux scaling for extremely overfilled apertures. The VSWF basis is convergent for fields which fall off to zero at large enough distances and thus can be truncated at some maximum mode, $n = n_{max}$. n_{max} is usually estimated with the function:

$$kr + 3\sqrt[3]{kr} \simeq n_{max} \tag{31}$$

for small objects and beams about a wavelength in size we need up to spherical harmonics up to $n \simeq 9$ [29, 30]. We can in turn estimate a good estimation of the field as a function of kr using this same relation. Root finding equation (31) we can in some sense relate the mode index $n^2 + (n + m)$ of the VSWF expansion to kr. We can observe the time averaged energy flux scaling behaviour by comparing different aperture sizes versus our truncation of wave functions. Figure 4(a) shows the suggested exponential behaviour for underfilled beams in small r limit and figure 4(b) shows the expected $1/kr$ energy flux fall-off for the real part of an $\mathrm{IG}_{\Lambda,i}$ (with $\Lambda = 5$, $i = 0$) beam with a convergence angle of 45°. Energy for time-harmonic waves is proportional to energy flux and thus could be used as a proxy here.

We would also like to verify that the diffraction generated by our computational model is representative of reality. To be able to simultaneously produce and measure the mode profile of the IG beam, a paraxial experimental apparatus (Mach–Zehnder interferometer) was constructed to interfere a reference wave with an apertured $\mathrm{IG}_{5,5}$ mode constructed from a 'complex' valued phase-only hologram [31]. The IG beam was generated using a device known as a spatial light modulator which is capable of producing controllable phase shifts to impinging light with micron scale resolution. By modulating the phase shift of the beam relative to the incident laser source a phase relationship between the different parts of the beam was established.

Figure 5(a) and (c) shows the theoretical prediction of the focal plane for the overfilled $\mathrm{IG}_{5,5}$ beam with a convergence angle of 22.5° and aperture truncation angle at 20°. It can be compared with a experimentally obtained paraxial simulation (using a much smaller convergence angle) to verify the edge diffraction as shown in figure 5(b) and (d). A convergence angle of 22.5° is sufficient to avoid most of the effects of non-paraxial wave propagation and so we expect to see broad agreement between the model and experimental paraxial result. The amplitude of the diffraction spots is small compared to the maximum amplitude. Our experimental paraxial result gives

a)

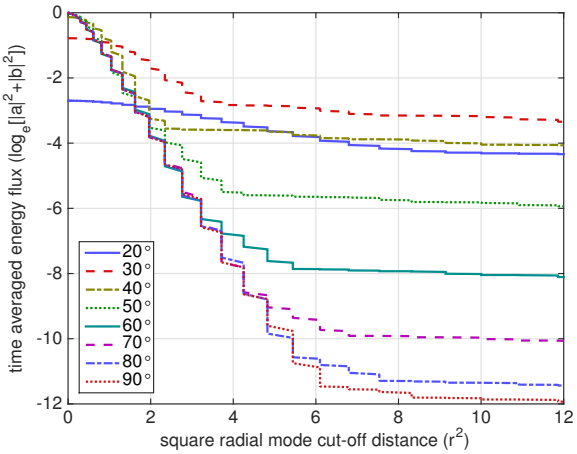

b)

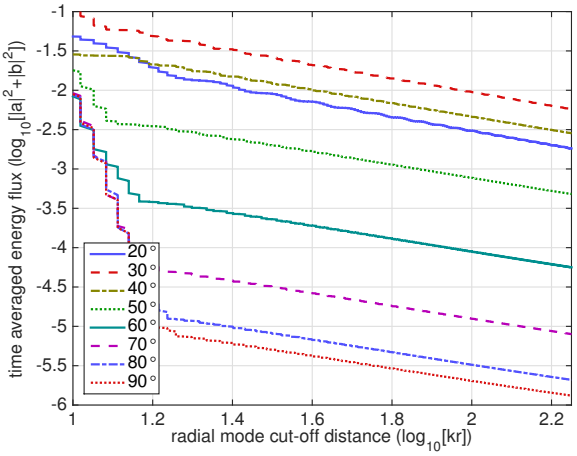

Figure 4: Absolute time averaged energy flux of the real part of the $IG_{5,5}$ beam (using the first row of $c_{5,2}$) with a convergence angle of 45° in the a) small, b) large radial mode (n) limits as an approximate function of a) r^2 and b) kr as determined by the truncation criteria. Each curve represents the energy flux for a given extent of the far-field aperture as a function of angle as shown in the legend. a) Linear-log plot of the energy flux. Exponential fall-off occurs in the low order radial modes approximately proportional to the argument of the Gaussian function, when the aperture is extremely overfilled the mode profile is no longer Gaussian and most of the energy flux falls outside the aperture as so the Gaussian energy flux distribution and amplitude is lost. b) Log-log plot of the energy flux. For the over-filled beams $1/kr$ dependence dominates the energy flux contribution at low degree radial modes. For larger apertures we see that $1/kr$ dependence occurs at larger radial modes.

reasonable agreement between the transverse amplitude profiles. The ripple in the amplitude profile reasonably matches the diffraction predicted by the computational method. Three strong fringes appear to either side of the profile corresponding to the part of the beam most strongly cut by the aperture. The phase profiles also give good agreement but vary due to the aberrations present in the optical system.

5 Momentum properties of Ince–Gaussian beams

The beam modes we have chosen to investigate have angular momentum in addition to linear momentum. It's well known that an extremely weakly focussed LG beam propagating along the z-axis has $(l + \sigma_z)\,\hbar$, angular momentum per photon where $l\hbar$ is the orbital angular momentum and $\sigma_z\hbar$ is the spin angular momentum. Knowing the precise superposition of LG modes to generate our vortex IG (vIG) modes means we can calculate the total torque for these beams using the transformation coefficients $c_{\Lambda,\xi}$:

$$\tau_i^{\mathrm{IG}} = \hbar k \left(\sigma_z + \sum_{j=0}^{\Lambda} \frac{2j - \Lambda}{\sqrt{2}} \left| c_{\Lambda,\xi}\left(i,j\right) \right|^2 \right). \tag{32}$$

Let us start with the orbital angular momentum of linearly polarised beam modes. Figure 6 shows the change in magnitude of angular momentum for a linearly polarised beam with variation of the ellipticity, ξ. Fractional angular momentum occurs in Ince–Gaussian beams due to local changes in phase gradients. Unlike the case for paraxial LG beams, the ratio of angular momentum density to energy density is not uniform over the beam cross-sections leading to fractional angular momentum.

In general the magnitude of angular momentum approaches a value near $\Lambda/2$ as ξ is increased, but this is not always the case and can be explained with reference to figure 7. The three panels in figure 7 tell the following story: as the ellipticity increases from 0 the vortex at the centre of the LG mode is destroyed and splits into charge 1 vortices spreading from the centre of the beam causing a reduction in the angular momentum. As the ellipticity parameter increases further, any line discontinuities split into vortices and as a result the angular momentum begins to increase. At extreme values of ellipticity the vortices cannot move apart any further and the angular momentum stabilises. This observation is consistent with that made in [25].

We can now study the spin component of the torque for vIG beams. It is well known that the σ_z component of a Gaussian beam is not invariant under focussing. However, we cannot change the total angular momentum of the beam unless we exert torque on the lens used to focus the beam. After traversing the lens the spin

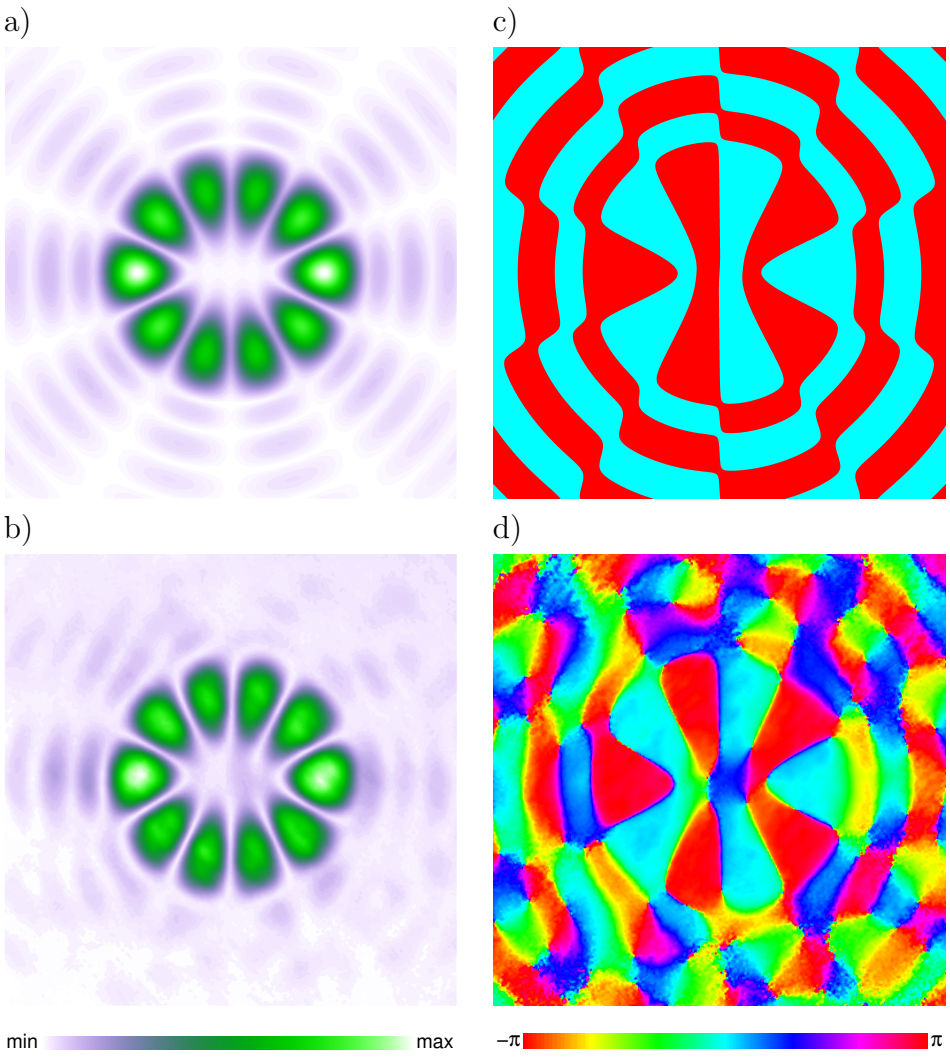

Figure 5: Amplitude and phase for the real part of an overfilled $IG_{5,5}$ beam with a convergence angle of 22.5° and aperture truncation angle of 20° determined from: The computational method for calculating diffracted modes in the high numerical aperture regime with a) amplitude and c) phase and the experimental b) amplitude and d) phase of the computational model. Diffraction is caused by cutting off the edges of the constituent LG modes during calculation. As VSWF should be a satisfactory model of tightly focussed beam modes the diffraction of the mode should be similar to actual observation. Experimental realisation of the computational model has reasonable agreement in both the high and low amplitude regions and phase given the presence of aberrations in the optical system.

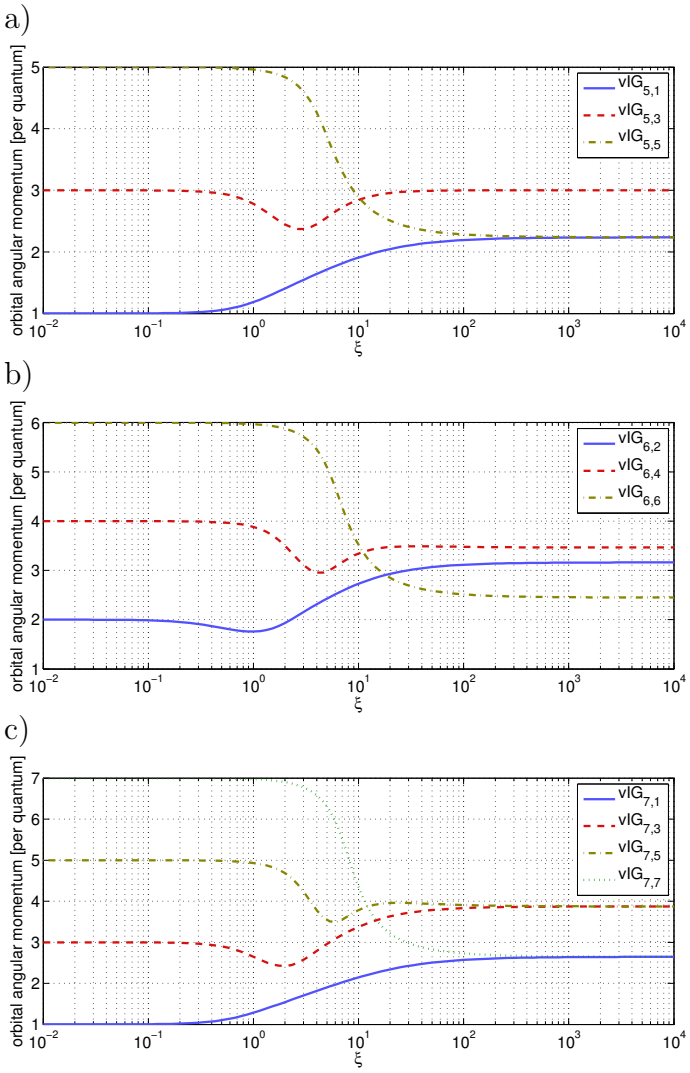

Figure 6: Orbital angular momentum for various vIG modes for degree, $\Lambda = 5, 6, 7$. Changing the ellipticity, ξ, changes the angular momentum (as measured around the beam propagation axis, 'z-axis') present in the resulting mode. The angular momentum of vIG matches the angular momentum eigenmode for $\xi = 0$. As $\xi \to \infty$ the angular momentum stabilises as ellipticity transforms from elliptical to Cartesian coordinates.

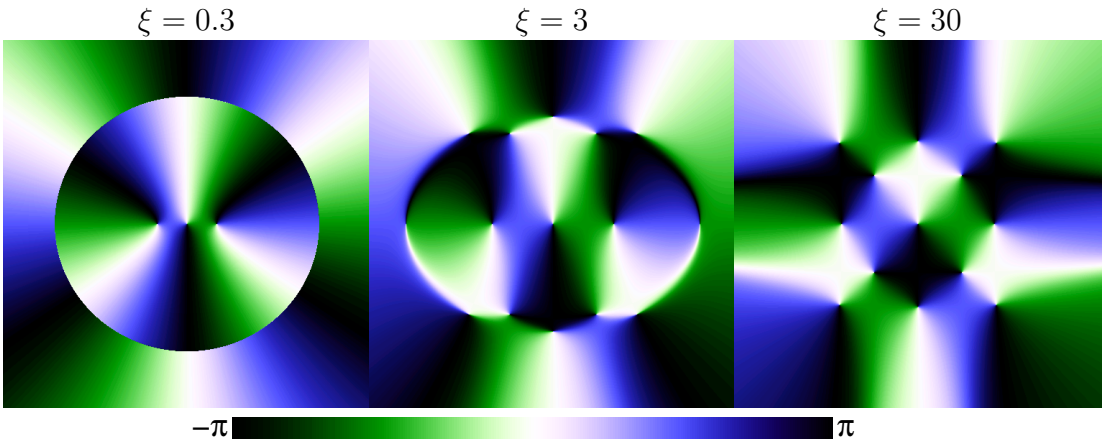

Figure 7: The transverse profile of the mode represented by the middle curve of figure 6(a) at the beginning, middle and end of the reduction of angular momentum at ellipticity: $\xi = 0.3$, $\xi = 3$, $\xi = 30$. These three panels tell the following story: as the ellipticity increases from 0 the central vortex is destroyed and splits into charge 1 vortices spreading from the centre of the beam causing a reduction in the angular momentum. As the ellipticity parameter increases further the line discontinuities split into vortices and as a result the angular momentum begins to increase. At extreme values of ellipticity the vortices cannot move apart any further and the angular momentum stabilises.

angular momentum can no longer be sufficiently quantified by the σ_z component [21]. Instead, part of the original spin angular momentum travels as orbital angular momentum. This is consistent with ray models of the contribution of spin angular momentum to the torque which have been shown to give excellent agreement with the electromagnetic theory of Gaussian beams. Figure 8 shows the correspondence between the ray model of the LG beam far-field and electromagnetic modelling (using the optical tweezers toolbox [11] to calculate the spin angular momentum from the mode amplitudes) as a function of beam convergence angle for one Gaussian mode and three mode profiles of paraxial degree 5, the LG modes: $\mathrm{LG}_{p,l}$, where $p = 0, 0, 1, 2$ corresponds to $|l| = 0, 5, 3, 1$. For energy flux normalised beams the ray theory exactly matches the electromagnetic theory. This should be the case as the ray picture in the far-field is not distinguishable from electromagnetic theory and should hold for the spin component of any mode. To calculate this for any given high-order Gaussian beam we need to take a mode weighted sum of the constituent modes (LG modes) to calculate the spin for that particular beam family. In general for a non-paraxial high-order Gaussian mode our total angular momentum per photon remains unchanged. However, our non-paraxial spin component does not and the following superposition:

$$\sigma_z^{(i)} = \sum_{j=0}^{\Lambda} \sigma_z^{(j)} \left| c_{\Lambda,\xi}\left(i,j\right)\right|^2, \tag{33}$$

needs to be evaluated.

The linear momentum of a tightly focussed beam can be calculated in the exact same manner as the spin angular momentum for a circularly polarised beam and should have the exact same magnitude. In the case of a weakly focussed Gaussian beam the linear momentum per photon should be close to the plane wave result: $\hbar k$ per photon. We therefore refer back to figure 8 for the quantity of linear momentum per photon along the propagation axis. Previously it was found that at a convergence angle of 90° both the spin angular momentum and linear momentum per photon has a minimum of $0.5\hbar k$ for a $\tan\theta$ (thin lens) aperture function. As a result it will not be the same as the prediction here which uses the more physical $\sin\theta$ aperture function found in equation (28). Therefore, our theoretical result for the momentum per photon for a Gaussian is approximately $0.68\hbar k$. We find that in general the linear and spin angular momentum for a high-order Gaussian beam is less than for a fundamental Gaussian mode. If we consider an infinitesimal ring we obtain momentum per photon of $\cos\theta$. This effect is therefore a predictable consequence of the increased angular distribution of light in higher-order Gaussian-type modes and large angle of incidence fields in general.

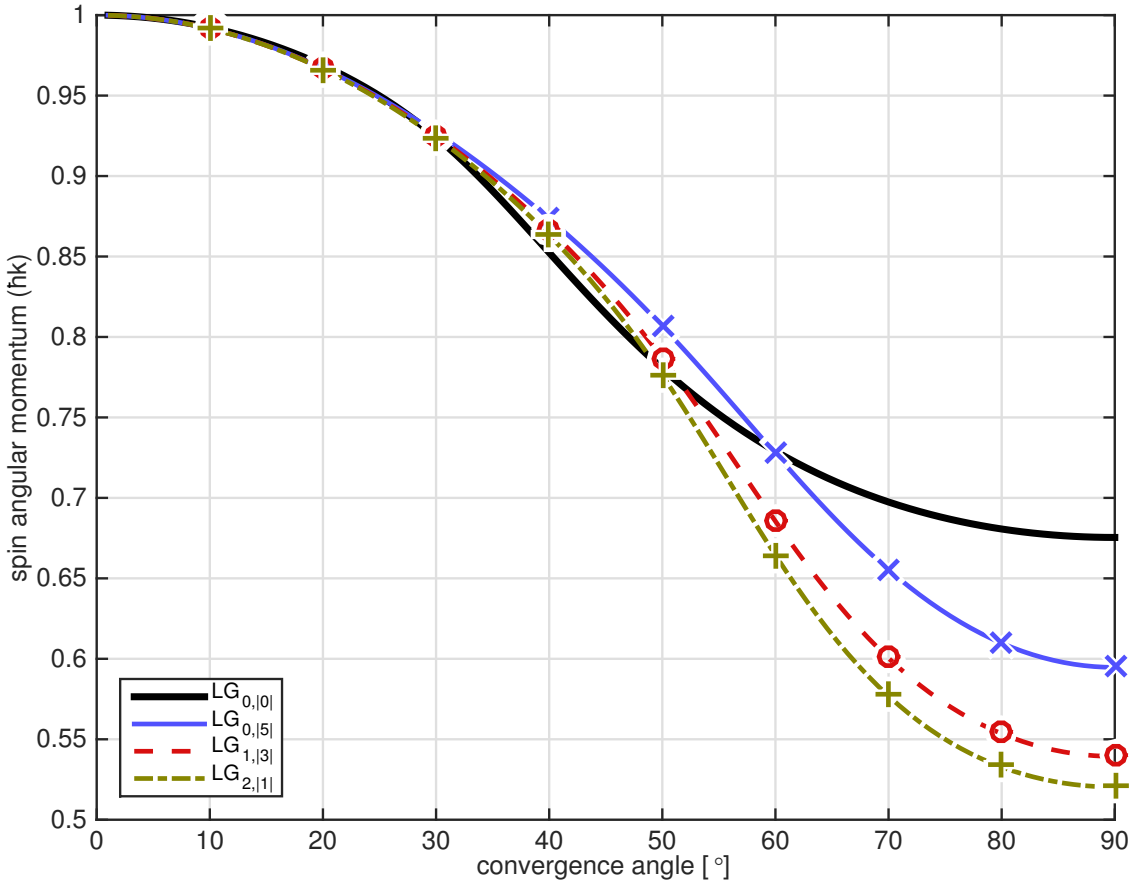

Figure 8: Spin angular momentum per photon (lines) with convergence angle for circularly polarised $\mathrm{LG}_{p,l}$ modes, where $p = 0, 0, 1, 2$ corresponds to $|l| = 0, 5, 3, 1$. The ray optics spin angular momentum calculation exactly matches the electromagnetic model (markers: $\times$, $\circ$, $+$) for every mode calculated.

6 Discussion and Conclusion

We have shown how arbitrary solutions of the paraxial wave equation can be expressed as a finite expansion of solutions to the vector Helmholtz wave equation in the presence of an aperture. Exact solutions are difficult to find for apertured systems so we have used a numerical model which means we have to meet truncation criteria to accurately reproduce paraxial-type modes using an electromagnetic analog. Our model is consistent with established theory and it displays *all* of the relevant optical physics including conservation of momentum, diffraction and angular momentum relations. The logarithm of energy flux distribution for Gaussian modes in our model is commensurate with r^{-2} for the first few dozen terms of our expansion and linear energy flux scaling with r^{-1} dominating for the remainder of the expansion due to edge effects from our simulated aperture. We conclude that an electromagnetic model of high-order Gaussian beams should not show any practical deviation from the ray optics predictions of the simple far-field properties of light (such as momentum per photon for uniformly polarised radiation). However, by using an electromagnetic model we can incorporate diffraction without any additional theory and have laid the foundations for the analysis of complex valued vector beam modes which cannot be easily modelled with either ray optics or scalar wave optics. It could provide insight into knotted light structures in the high NA regime as the VSWFs are a natural vortex-bearing basis. The method chosen is based on a modal representation which makes it highly compatible with scattering matrix representations of particles and matter. Therefore, our model and method has great potential application for analysis of optical micromanipulation in complex light fields such as those found in particle sorting and tweezers-stimulated structure formation.

Acknowledgements

Thanks to Andrew G. White for useful discussions on paraxial beam mode transformations. Thanks to Christina Alpmann for general discussions about Ince–Gaussian beams. This work is supported by Australian Research Council Discovery Grant DP1095880.

References

[1] Mike Woerdemann, Christina Alpmann, Michael Esseling, and Cornelia Denz. Advanced optical trapping by complex beam shaping. *Laser & Photonics Re-*

views, 7(6):839–854, 2013.

[2] David L Fried and Jeffrey L Vaughn. Branch cuts in the phase function. *Applied Optics*, 31(15):2865–2882, 1992.

[3] Mark R Dennis, Robert P King, Barry Jack, Kevin O'Holleran, and Miles J Padgett. Isolated optical vortex knots. *Nature Physics*, 6(2):118–121, 2010.

[4] Miguel A Bandres and Julio C Gutiérrez-Vega. Ince Gaussian beams. *Optics letters*, 29(2):144–146, 2004.

[5] Philip McCord Morse and Herman Feshbach. *Methods of Theoretical Physics*. McGraw-Hill, New York, 1953.

[6] M. I. Mishchenko. Light scattering by randomly oriented axially symmetric particles. *Journal of the Optical Society of America A*, 8(6):871–882, 1991.

[7] J. Stratton. *Electromagnetic Theory*. McGraw-Hill, New York, 1941.

[8] Milton Abramowitz and Irene A. Stegun, editors. *Handbook of Mathematical Functions With Formulas, Graphs, and Mathematical Tables*. National Bureau of Standards, Washington D.C., 1972.

[9] Gabriel Molina-Terriza. Determination of the total angular momentum of a paraxial beam. *Physical Review A*, 78(5):053819, 2008.

[10] T. A. Nieminen, H. Rubinsztein-Dunlop, and N. R. Heckenberg. Multipole expansion of strongly focussed laser beams. *Journal of Quantitative Spectroscopy and Radiative Transfer*, 79-80:1005–1017, 2003.

[11] T. A. Nieminen, V. L. Y. Loke, A. B. Stilgoe, G. Knöner, A. M. Brańczyk, N. R. Heckenberg, and H. Rubinsztein-Dunlop. Optical tweezers computational toolbox. *Journal of Optics A: Pure Applied Optics*, 9:S196–S203, 2007.

[12] Ø. Farsund and BU Felderhof. Force, torque, and absorbed energy for a body of arbitrary shape and constitution in an electromagnetic radiation field. *Physica A*, 227(1-2):108–130, 1996.

[13] J. H. Crichton and P. L. Marston. The measurable distinction between the spin and orbital angular momenta of electromagnetic radiation. *Electronic Journal of Differential Equations*, Conf. 04:37–50, 2000.

[14] E. Abramochkin and V. Volostnikov. Beam transformations and nontransformed beams. *Optics Communications*, 83(1–2):123 – 135, 1991.

[15] M. W. Beijersbergen, L. Allen, H. Van der Veen, and J. P. Woerdman. Astigmatic laser mode converters and transfer of orbital angular momentum. *Optics Communications*, 96(1-3):123–132, 1993.

[16] Isidoro Kimel and Luis R Elias. Relations between Hermite and Laguerre Gaussian modes. *IEEE Journal of Quantum Electronics*, 29(9):2562–2567, 1993.

[17] Miguel A. Bandres and Julio C. Gutiérrez-Vega. Ince–Gaussian modes of the paraxial wave equation and stable resonators. *J. Opt. Soc. Am. A*, 21(5):873–880, May 2004.

[18] Herbert G Winful et al. Physical origin of the Gouy phase shift. *Optics letters*, 26(8):485–487, 2001.

[19] Les Allen, M W Beijersbergen, R J C Spreeuw, and J P Woerdman. Orbital angular momentum of light and the transformation of Laguerre-Gaussian laser modes. *Physical Review A*, 45(11):8185–8189, 1992.

[20] J. Courtial and M.J. Padgett. Limit to the orbital angular momentum per unit energy in a light beam that can be focussed onto a small particle. *Optics communications*, 173(1):269–274, 2000.

[21] T. A. Nieminen, A. B. Stilgoe, N. R. Heckenberg, and H. Rubinsztein-Dunlop. Angular momentum of a strongly focused Gaussian beam. *Journal of Optics A: Pure and Applied Optics*, 10:115005, 2008.

[22] Yiqiong Zhao, J. Scott Edgar, Gavin D. M. Jeffries, David McGloin, and Daniel T. Chiu. Spin-to-orbital angular momentum conversion in a strongly focused optical beam. *Phys. Rev. Lett.*, 99:073901, Aug 2007.

[23] Luiz F Roncaratti and Vincenzo Aquilanti. Whittaker–Hill equation, Ince polynomials, and molecular torsional modes. *International Journal of Quantum Chemistry*, 110(3):716–730, 2010.

[24] E. L. Ince. A linear differential equation with periodic coefficients. *Proceedings of the London Mathematical Society*, 2(1):56–74, 1925.

[25] William N. Plick, Mario Krenn, Robert Fickler, Sven Ramelow, and Anton Zeilinger. Quantum orbital angular momentum of elliptically symmetric light. *Phys. Rev. A*, 87:033806, Mar 2013.

[26] Dmitriĭ Aleksandrovich Varshalovich, Anatolij Nikolaevič Moskalev, and Valerij Kel'manovĭc Khersonskii. *Quantum theory of angular momentum*. World Scientific, Singapore, 1989.

[27] Morris E Rose. *Elementary theory of angular momentum*. John Wiley & Sons, New York, 1957.

[28] Alan Robert Edmonds. *Angular momentum in quantum mechanics*. Princeton University Press, USA, 1996.

[29] J.H. Bruning and Yuen Lo. Multiple scattering of EM waves by spheres part I–Multipole expansion and ray-optical solutions. *Antennas and Propagation, IEEE Transactions on*, 19(3):378–390, May 1971.

[30] Billy C. Brock. *Using Vector Spherical Harmonics to Compute Antenna Mutual Impedance from Measured or Complex Fields*. Sandia National Laboratories, 2001.

[31] Joseph P. Kirk and Alan L. Jones. Phase-only complex-valued spatial filter. *J. Opt. Soc. Am.*, 61(8):1023–1028, Aug 1971.